Profile cutting on alumina ceramics by abrasive waterjet. II. Cutting performance models

Author/Contributor:
Wang, Jun; Liu, Hua

Publication details:
Proceedings of the Institution of Mechanical Engineers, Part C: Journal of Mechanical Engineering Science
v. 220
Chapter No. 5
pp. 715-725
0954-4062 (ISSN)

Publication Date:
2006

Publisher DOI:
http://dx.doi.org/DOI:10.1243/09544062JMES207B

Proceedings of the Institution of Mechanical Engineers
Part C Journal of Mechanical Engineering Science
Vol. 220, 2006, pp. 715-725

Profile cutting on alumina ceramics by abrasive waterjet. II. Cutting performance models

J. Wang* and H. Liu
School of Mechanical and Manufacturing Engineering, The University of New South Wales, Sydney, Australia

Abstract: Predictive models for the major cutting performance measures, such as the kerf taper and depth of cut, are developed for both straight-slit cutting and profile cutting by an abrasive waterjet (AWJ). The plausibility and predictive capability of the models are assessed and verified by comparing the model predictions with the corresponding experimental data. Very good correlations between the predicted and experimental results have been found, which confirms the adequacy of the models for use in process planning.

Keywords: Abrasive waterjet; AWJ; Profile cutting; Cutting performance; Cutting performance model; AWJ cutting

NOTATION

d_j	nozzle diameter (mm)
d_p	average particle diameter (mm)
σ	material flow stress (MPa)
h	depth of cut in straight cutting (mm)
h_r	depth of cut in contouring (mm)
h_s	smooth depth of cut (mm)
C's, k's, a's, b, c	constants
m_a	abrasive mass flow rate (g/s)
m_p	average mass of a particle (g)
m_w	water mass flow rate (g/s)
n	number of particles
P	water pressure (MPa)
R	profile curvature radius (mm)
S_d	standoff distance (mm)
u	nozzle traverse speed (mm/s)
u_j	waterjet velocity before mixing with particles (m/s)
u_p	particle velocity (m/s)
V_t	total material removal rate (mm^3/s)
V_s	volume of material removed by a particle (mm^3/s)
w	average kerf width (mm)
w_t	top kerf width (mm)
α	particle attack angle (degrees)
θ	kerf taper angle (degrees)
ρ_p	particle density (kg/m^3)
ρ_w	water density (kg/m^3)

* Corresponding author: Fax: +61-2-9663 1222, Email: jun.wang@unsw.edu.au (J. Wang).

1 INTRODUCTION

In the first part of this investigation [**1**] an experimental study of the cutting performance when profile cutting on an alumina ceramic by an abrasive waterjet (AWJ) is presented. It has been found that the radius of the profile curvature in AWJ profile cutting has a profound effect on the geometrical errors of the kerf walls. The kerf taper angles on the two kerf walls produced in AWJ profile cutting are different in magnitude and exhibit different trends when the profile curvature changes. It has also been found that the depth of cut is affected by the profile curvature. It increases with an increase in the radius of the profile curvature and approaches its maximum in straight-slit cutting. In process planning, it is essential to quantitatively predict these and other major kerf geometrical characteristics for the optimum selection of process parameters, and for compensating for kerf geometrical defects such as kerf tapers by using a correct jet side impact angle.

In this paper, predictive models for AWJ straight cutting and profile cutting are developed for the major cutting performance measures, i.e. the kerf taper angles and depth of cut, using a dimensional analysis method. Models for the other cutting performance measures (top kerf width and smooth depth of cut) are also developed using the experimental data obtained in the first part of this investigation. The plausibility and predictive capability of the model are then assessed by qualitatively and quantitatively comparing the model predictions with the corresponding experimental results.

2 PREDICTIVE MODELS FOR KERF TAPER ANGLES

2.1 Model formulation

Kerf taper is an important kerf geometrical feature in AWJ machined parts and needs to be controlled to within the tolerance limit. Moreover, in order to meet this component quality requirement, an appropriate action may be taken to compensate for the kerf taper. For these purposes, predictive models for this cutting performance measure are required. As mentioned in the first part of this investigation [**1**], kerf taper angles on the two kerf walls are not in the same magnitude in AWJ profile-cutting and need to be considered separately when developing predictive models.

The AWJ cutting process involves a large number of parameters that affect the cutting performance, such as the depth of cut and kerf tapers. In addition, a number of phenomena, such as particle interference and fragmentation, exist in AWJ cutting. At this stage of development, there is no sufficient knowledge of these phenomena [**2**, **3**]. Therefore, to consider all these variables and phenomena is either impossible or results in many unknown parameters in the final equation, making the model too complicated or unrealistic for practical use. In the present study, a dimensional analysis technique will be used to develop the kerf taper angle in this section and the depth of cut model in the next section, where the experimental data obtained in the first part of this investigation [**1**] will be used to allow for the other phenomena that cannot be mathematically expressed at this stage. The models for straight-slit cutting will be developed first, based on which the models for profile cutting are then developed.

Fundamentally, the magnitude of kerf taper angle is related to the jet effective diameter which decreases as the jet cuts into a workpiece. Within the effective diameter, the particle energy is sufficient for removing the target material. It has been reported [**4**] that the jet effective diameter depends on the water pressure and its distribution, standoff distance, nozzle diameter, and material destructive energy. Accordingly, these factors need to be considered in modelling kerf taper angles. In this work, material flow stress σ is selected to represent material properties. Furthermore, kerf taper is affected by nozzle traverse speed as a result of the number of particles impacting on a given exposed surface [**5**, **6**]. It has also been reported

that to some extent, abrasive mass flow rate affects the kerf taper angle [**1**, **7**]. As the number of particles is related to the abrasive mass flow rate for given particle size and density, it may be used to represent the abrasive mass flow rate in a particular operation. Consequently, kerf taper angle can be written as a function of water pressure *P*, nozzle traverse speed *u*, standoff distance S_d, nozzle diameter d_j, number of particles *n*, and material flow stress σ, such that

$$\theta = f\left(P, u, n, S_d, d_j, \sigma\right) \tag{1}$$

A dimensional analysis technique [**8**] is now employed to establish the relationship of kerf taper angle and the process variables in Eq. (1). With this technique, all variables appearing in a problem can be assembled into a smaller number of independent dimensionless *pi* (π) groups or products using the constraint that all products formed must have the same dimension. The relations connecting the individual variables can be determined by algebraic expressions relating each dimensionless product [**8**, **9**]. It is noticed in Eq. (1) that θ is a dimensionless variable, while all other variables in the equation depend on three fundamental dimensions, i.e. length *L*, mass *M* and time *T*. Using the dimensional analysis method, three repeating variables, d_j, *P*, and *u* are selected to form the *pi* groups, so that four *pi* groups (seven variables in Eq. (1) minus three repeating variables) can be established. Since θ is already a dimensionless variable and can form a product on its own, three more independent dimensionless products can be formed. The four dimensionless products are given by

$$\pi_1 = \theta \tag{2}$$

$$\pi_2 = \frac{\sigma}{P} \tag{3}$$

$$\pi_3 = \frac{u}{n\, d_j} \tag{4}$$

$$\pi_4 = \frac{S_d}{d_j} \tag{5}$$

where *n* is the number of particles supplied to the jet in a unit time and is given by

$$n = \frac{m_a}{m_p} \tag{6}$$

in which m_a is abrasive mass flow rate and m_p is the average mass of an abrasive particle. If assuming that the shape of the particles is spherical, the mass of a particle can be given by

$$m_p = \frac{\pi}{6} d_p{}^3 \rho_p \tag{7}$$

Other parameters are as defined in the Notation. Therefore, kerf taper angle can be expressed by

$$\theta = f\left(\frac{\sigma}{P}, \frac{u}{n\, d_j}, \frac{S_d}{d_j}\right) \tag{8}$$

Applying the power law function to Eq. (8) gives

$$\theta = a_0 \left(\frac{\sigma}{P}\right)^{a_1} \left(\frac{u}{n\, d_j}\right)^{a_2} \left(\frac{S_d}{d_j}\right)^{a3} \tag{9}$$

where a_0 to a_3 are coefficients. By regression analysis of the experimental data obtained in the first part of this investigation [**1**] at a 95% confidence level, the coefficients have been

determined. Taking $n=m_a/m_p$ from Eq. (6), the resulting predictive model for the kerf taper angle for AWJ straight cutting is given by

$$\theta = 0.156 \left(\frac{\sigma}{P}\right)^{0.633} \left(\frac{u\, m_p}{m_a\, d_j}\right)^{0.227} \left(\frac{S_d}{d_j}\right)^{0.39} \tag{10}$$

Re-arranging Eq. (10) and considering Eq. (7) gives

$$\theta = 0.135 \frac{\sigma^{0.633}\, u^{0.227}\, S_d{}^{0.39}\, d_p{}^{0.681} \rho_p{}^{0.227}}{P^{0.633}\, m_a{}^{0.227}\, d_j{}^{1.39}} \tag{11}$$

where u is in mm/s, S_d, d_p, and d_j are in mm, m_a is in g/s, ρ_p is in kg/m^3, P and σ are in MPa, and θ is in degrees.

The experimental investigation of profile cutting presented in part one of this investigation [**1**] has shown that kerf taper angles on the two kerf walls are different in magnitude and that the one on the convex side of the kerf wall decreases with an increase in the radius of profile curvature of the cut, while that on the concave side increases. To consider the effect of the profile curvature on the kerf taper angles, a proportionality factor is introduced for the convex and concave kerf walls respectively, so that the equations for kerf taper angles in AWJ profile-cutting become

$$\theta_{convex} = k_1\, \theta \tag{12}$$

$$\theta_{concave} = k_2\, \theta \tag{13}$$

where k_1 and k_2 are constant and have been statistically determined from the experimental data for 87% alumina ceramics at a 95% confidence level. The resulting models for the kerf taper angles on the convex and concave sides of the kerf walls are respectively given by

$$\theta_{convex} = \left(1 + \frac{1}{6.4124 + 0.1175\, R^{1.1591}}\right)\theta \tag{14}$$

$$\theta_{concave} = \left(1 - \frac{1}{3.0112 + 0.0445\, R^{1.1576}}\right)\theta \tag{15}$$

where R is in mm, θ_{convex}, $\theta_{concave}$ and θ are in degrees, and θ can be found from Eq. (11).

3.2 Model assessment

The generality and plausibility of the models for kerf taper angles in AWJ straight cutting and profile cutting are examined by analysing the predicted trends with respect to the process parameters, as shown in Figs. 1 and 2, where the lines represent the predicted values and the symbols are for the experimental results. It can be noticed that the kerf taper angles on the two kerf walls in AWJ straight cutting and profile cutting increase with an increase in the standoff distance and nozzle traverse speed, and decreases with an increase in water pressure. Abrasive flow rate shows only a marginal effect on the kerf tapers. The profile curvature has caused a deviation between the kerf tapers on the two kerf walls, but their difference decreases as the radius of the profile curvature increases. Qualitatively, the model's predictions are reasonable, which confirms that the developed models have been formulated correctly.

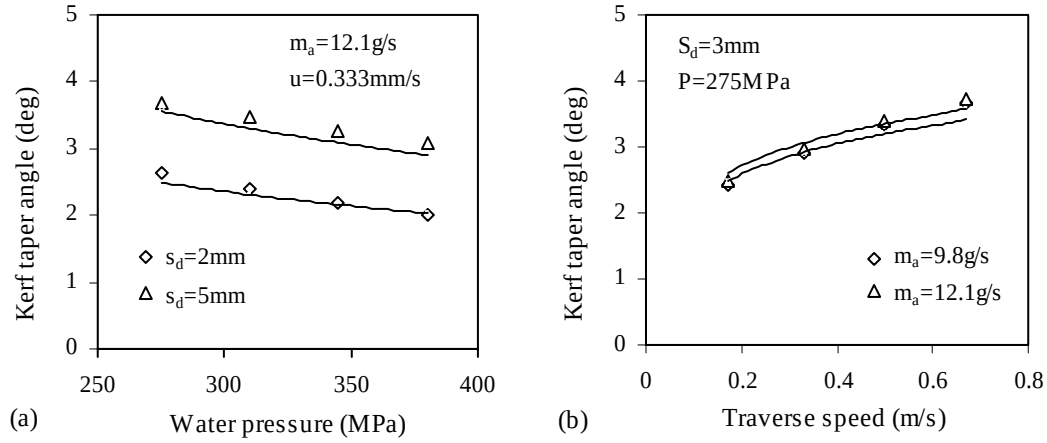

Fig. 1 Predicted trends for kerf taper angle in AWJ straight cutting

As shown in Fig. 2(a), the predicted trends for kerf taper angles on the convex side of kerf walls decreases with an increase in the radius of profile curvature, while a reverse trend is seen on the concave side. This trend is caused by the jet which changes its direction towards the concave side of the kerf wall when it cuts into the workpiece, and hence cuts more material from the concave side than from the convex side of the kerf wall in profile cutting. The difference between the two kerf taper angles decreases with an increase in the profile radius. The models have correctly predicted these trends.

Fig. 2(b) shows that the kerf taper angles on the two kerf walls increase with an increase in standoff distance in AWJ profile cutting. This is consistent with the experimental data represented by the symbols. A similar trend can be seen in Fig. 1(a) for straight cutting. This trend may be attributed to the fact that the jet diameter increases as the jet flows away from the nozzle exit and the effective jet diameter at the workpiece surface may also increase as the standoff distance increases, opening a wider entry slot. However, the effective jet diameter at the lower part of the material is reduced because of the increase in standoff distance. The combined effect results in an increase in the kerf taper angle. This trend has again been correctly predicted by the models for both straight and profile cutting.

The predicted kerf taper angles increase with an increase in nozzle traverse speed as shown in Fig. 1(b) as well as in Fig. 2(c). A faster passage of the abrasive waterjet allows fewer particles to strike on the target material, hence decreasing the kerf width. However, as the jet loses its energy when cutting into the workpiece, the kerf width at the lower part of the cutting front decreases even more than the top kerf, resulting in an increase in the kerf taper angles, as indicated by the experimental data in the figure. The models have correctly predicted this trend.

The predicted relationship between water pressure and kerf taper is shown in Fig. 2(d). It can be seen that the kerf taper angles on the two kerf walls decrease monotonically with an increase in water pressure. A similar trend is also found in Fig. 1(a) for straight cutting. From the experimental data in this investigation, the top kerf width remains relatively constant as the water pressure changes while the width at a lower part of the kerf increases steadily with water pressure due to the increased effective jet diameter by the increased water pressure. The combination of these effects results in a decrease in the kerf taper angle as water pressure increases. The predicted trend correlates very well with the experimental findings as shown by the data plotted in the figure.

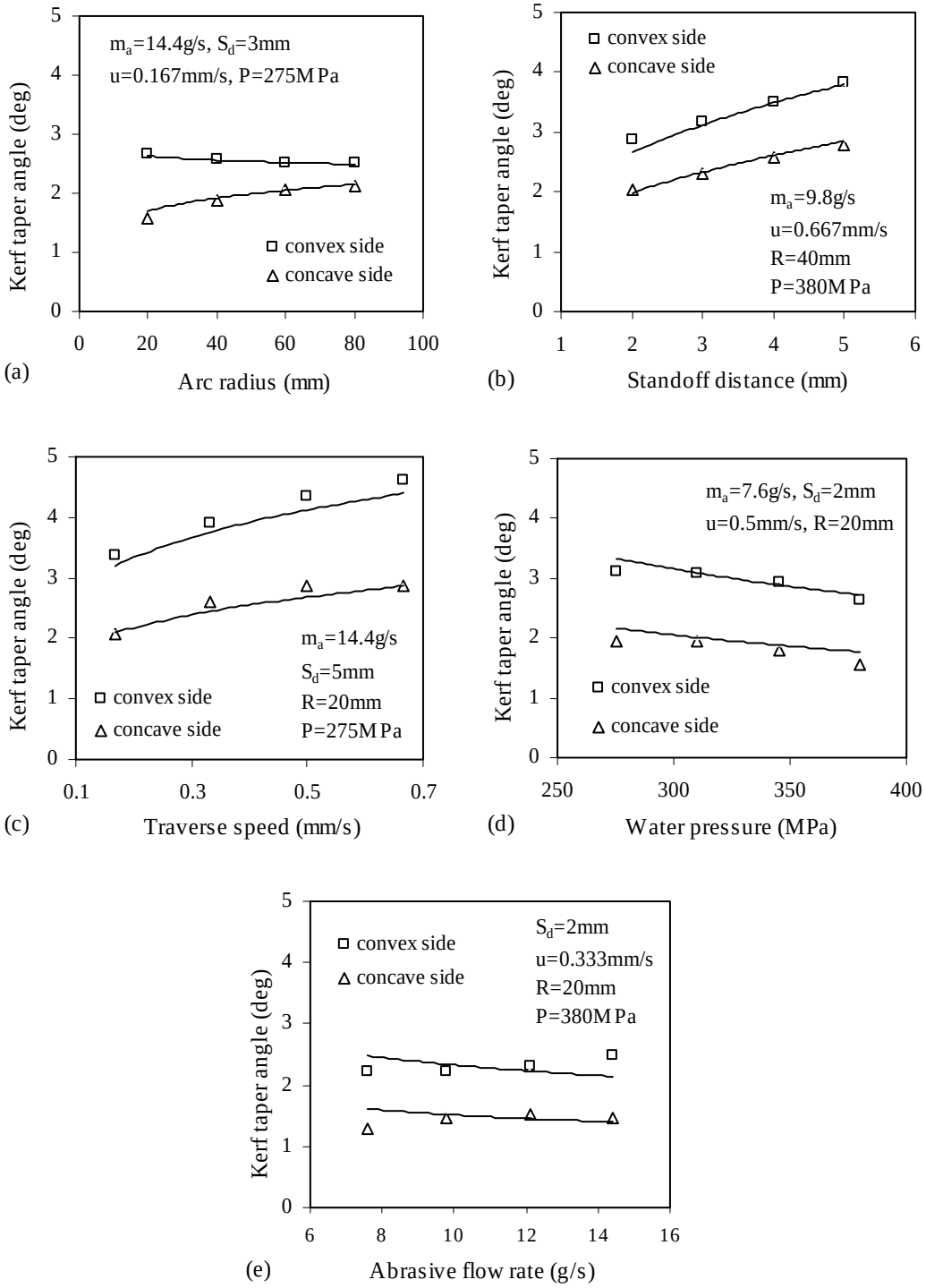

Fig. 2 Predicted trends for kerf taper angle in AWJ profile cutting

The kerf tapers show a marginal decrease with an increase in abrasive flow rate, as shown in Figs. 1(b) and 2(e) for AWJ straight cutting and profile cutting respectively. The figures also show that kerf tapers on both the convex and concave sides of the kerf walls decrease in a similar manner, suggesting that the difference of kerf taper angles on the two kerf walls is caused by the kerf curvature only. While this may be anticipated from the experimental investigation, the results have again confirmed that the forms of the developed models are indeed correct.

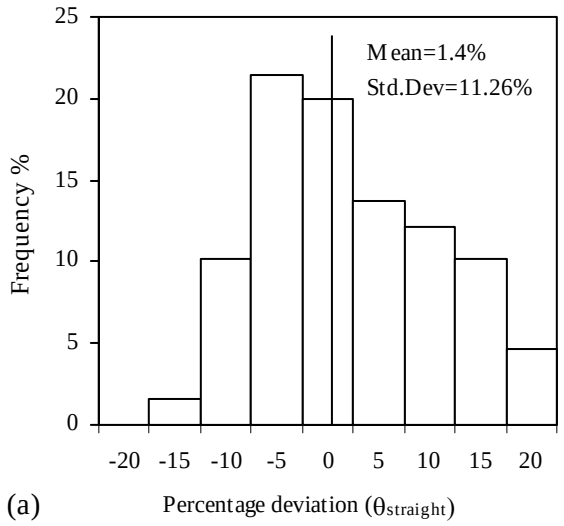

(a)

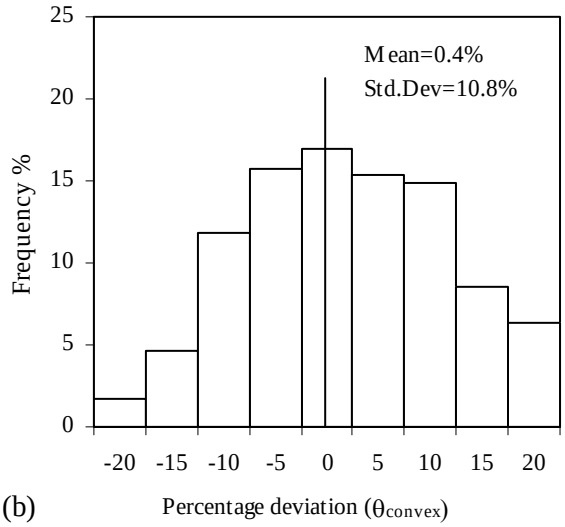

(b)

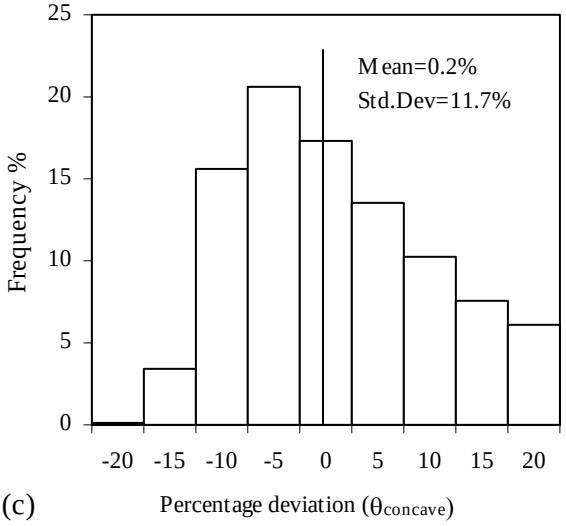

(c)

Fig. 3 Percentage deviations of predicted kerf taper angles from experimental data: (a) Straight cutting, (b) Convex side in profile cutting, (c) Concave side in profile cutting

The adequacy of the models is examined quantitatively by comparing the percentage deviations of the model predicted values with the corresponding experimental data using the following equation

$$\%\text{dev.} = \frac{\text{Predicted result} - \text{Experimental result}}{\text{Experimental result}} \times 100\% \quad (16)$$

These quantitative comparisons are given in Fig. 3. It is noted that for straight cutting as shown in Fig. 3(a), the average percentage deviation of the model predictions from the corresponding experimental data is 1.4% with a standard deviation of 11.26%. The histogram in Fig. 3(b) shows that the model prediction gives an average percentage derivation of 0.4% with the standard deviation of 10.8% for kerf taper angles on the convex side of kerf wall in profile cutting. The corresponding deviations for the taper angles on the concave side are 0.2% on average and 11.7% for the standard deviation, as shown in Fig. 3(c). These quantitative comparisons have shown that the developed models can provide adequate predictions for kerf taper angles in practical AWJ cutting of 87% alumina ceramics.

3 PREDICTIVE MODELS FOR THE DEPTH OF CUT

3.1 Model formulation

For the same reasons as mentioned in Section 2 of this paper, the dimensional analysis technique will be used and an attempt will be made on the straight-slit cutting first, before considering the depth of cut in profile cutting.

In AWJ cutting, the material removal rate, V_t, can be expressed as a function of the cross-section area of the cutting front (depth of cut, h, multiplying kerf width, w) and jet traverse (or feed) speed, u, namely

$$V_t = h\, w\, u \quad (17)$$

By ignoring the variation of kerf width along the depth, and assuming that the kerf width is equal to the effective jet diameter (within which the particles have energy above the threshold value for removing the target material), which is in turn assumed to be equal to the nozzle diameter, d_j, Eq. (17) becomes

$$V_t = h\, d_j\, u \quad (18)$$

Consequently, the depth of cut for AWJ straight cutting can be given by

$$h = \frac{V_t}{d_j\, u} \quad (19)$$

The material removed in AWJ cutting may be considered as an accumulation of material removed by numerous individual particles. Thus, the material removal rate may be expressed by

$$V_t = C_0\, n\, V_s \quad (20)$$

where V_s is the volume of material removed by a single particle, C_0 is an efficiency factor to allow for the fact that not all particles are involved in the erosion process and some particles do not have sufficient energy to cut the material, and n is the number of particles supplied to the jet in a unit time and can be found from Eq. (6).

It is now essential to develop the volume of material removed by a single particle V_s. It has been established that the erosion process of brittle materials, such as ceramics, is controlled by the formation and propagation of cracks [**10**, **11**]. The material volume removal by a single particle can be estimated in terms of the target material properties (fracture toughness, hardness, flow stress etc.) and particle properties represented by velocity, density, shape and

size [**12**, **13**]. However, it is not realistic to include all material properties in modelling the AWJ cutting performance. Thus only the major and typical variables are considered. In this work, the volume removal by a single particle is considered as a function of particle mass, m_p, particle velocity u_p, local particle attack angle, α, and the flow stress of target material, σ, and can be expressed in the following form

$$V_s = \phi(m_p, u_p, \alpha, \sigma) \tag{21}$$

By using the dimensional analysis technique [**8**], all the variables in Eq. (21) depend on three fundamental dimensions, i.e. length *L*, mass *M* and time *T*. With these three fundamental dimensions, two *pi* groups or products can be formed from Eq. (21) with five variables. Since α is already a dimensionless variable, one more independent dimensionless product can be formed and the two products are given by

$$\pi_1 = \frac{V_s \sigma}{m_p u_p^{\,2}} \tag{22}$$

$$\pi_2 = \alpha \tag{23}$$

Applying the functional relationship between these two products and the power law formulation, the dimensional equation is given by

$$V_s = C_1 \frac{m_p u_p^{\,2}}{\sigma} \alpha^a \tag{24}$$

It is assumed that the particles are uniformly distributed along the jet and particle velocity variation along the jet can be ignored. It is further assumed that the velocity of particles is equal to that of their surrounding water. Thus, the particle velocity can be obtained using the momentum transfer equation, i.e.

$$u_p = k_1 \left(\frac{m_w}{m_w + m_a} \right) u_j \tag{25}$$

where u_j is the waterjet velocity before it is mixed with abrasives, m_w is the water mass flow rate, and k_1 is a factor to consider the momentum transfer efficiency. The particle velocity, u_p, is assumed to be the velocity of the water-particle slurry jet. To work out the mass ratio term in Eq. (25) will make the model complicated. Therefore, the ratio term is approximated by a constant, k_2, to simplify the derivation. For the process conditions used in the experiments given in the first part of this investigation, this approximation only results in less than 2.5% error for the mass ratio and even smaller error for the final depth of cut. Thus, Eq. (25) can be re-written as

$$u_p = k_1 \, k_2 \, u_j \tag{26}$$

If assuming that the energy loss in the system is negligible, the velocity of waterjet, u_j, can be found by using the Bernoulli's equation, i.e.

$$u_j = \sqrt{\frac{2P}{\rho_w}} \tag{27}$$

where *P* is water pressure and ρ_w is water density. Substituting Eqs. (26) and (27) into Eq. (24) gives

$$V_s = C_1 \frac{m_p (k_1 k_2)^2 (2P)}{\rho_w \sigma} \alpha^a \tag{28}$$

The magnitude of the local particle attack angle, α, varies as the depth of cut increases. However, the exact nature of this variation is not clear and an extensive literature review did

not reveal any viable or practical models to describe this angle [**14**, **15**]. Thus, the average particle attack angle is used in this study and its value is determined by a dimensional analysis technique. According to the reported investigations [**16**, **17**], the jet attack angle depends on the profile of the cutting front which in turn depends on the jet traverse speed, u, abrasive flow rate, m_a, material flow strength, σ, and the jet diameter. It is assumed that the jet diameter is approximately equal to the nozzle diameter, d_j. For given abrasive particles (or particle density and size), the abrasive flow rate, m_a, may be represented by the number of particles, n. Furthermore, water pressure, P, is related to the water and particle velocity in a jet and affects material removal and particle flow direction. Therefore, water pressure is included in the analysis. Thus, the average particle attack angle is given by

$$\alpha = \varphi(P, u, n, d_j, \sigma) \tag{29}$$

Using the dimensional analysis technique, three independent dimensionless groups can be formed; namely,

$$\pi_1 = \frac{\sigma}{P} \tag{30}$$

$$\pi_2 = \frac{u}{n\, d_j} \tag{31}$$

$$\pi_3 = \alpha \tag{32}$$

The three groups are related by the function

$$\pi_3 = \varphi(\pi_1, \pi_2) \tag{33}$$

Applying the power law formulation gives

$$\alpha = C_2 \left(\frac{\sigma}{P}\right)^b \left(\frac{u}{n\, d_j}\right)^c \tag{34}$$

Consequently, by substituting Eqs. (6) and (28) into Eq. (20) with the particle attack angle found from Eq. (34), the general form of material removal rate can be given by

$$V_t = C \frac{m_a P}{\rho_w \sigma} \left(\frac{\sigma}{P}\right)^{a_1} \left(\frac{\pi d_p{}^3 \rho_p u}{6 m_a d_j}\right)^{a_2} \tag{35}$$

where C, a_1 and a_2 are contacts introduced to generalise the other constants. From Eq. (19), the depth of cut equation for straight-slit cutting can be given by

$$h = C \frac{m_a P}{\rho_w \sigma u d_j} \left(\frac{\sigma}{P}\right)^{a_1} \left(\frac{\pi d_p{}^3 \rho_p u}{6 m_a d_j}\right)^{a_2} \tag{36}$$

Eq. (36) may be considered as the general form of the depth of cut equation for brittle materials in which the constants can be obtained by regression analysis of the test data when cutting a brittle material under consideration. For the 87% alumina ceramics used in this investigation, the constants were statistically determined from the experimental data at a 95% confidence level, so that the depth of cut model becomes

$$h = 5362.77 \frac{m_a P}{\rho_w \sigma u d_j} \left(\frac{\sigma}{P}\right)^{0.735} \left(\frac{\pi d_p{}^3 \rho_p u}{6 m_a d_j}\right)^{0.895} \tag{37}$$

By re-arranging Eq. (37), the depth of cut equation can be given by

$$h = 3005.33 \frac{m_a^{0.105} P^{0.265} \rho_p^{0.895} d_p^{2.685}}{u^{0.105} \rho_w \sigma^{0.265} d_j^{1.895}} \quad (38)$$

where h, d_p and d_j are in mm, m_a is in g/s, u is in mm/s, ρ_w and ρ_p are in kg/m^3, P and σ are in MPa.

It has been reported in the first part of this investigation [**1**] that the depth of cut in AWJ profile cutting increases with the radius of profile curvature and approaches its maximum value when straight-cutting. To consider the effect of profile curvature when developing the depth of cut model for profile cutting or contouring, a proportionality factor, k, is introduced. Thus the depth of cut for contouring, h_r is

$$h_r = k\,h \quad (39)$$

where the proportionality factor can be determined from the experimental data. For the 87% alumina ceramics used in this study, the depth of cut model for AWJ profile cutting is given by

$$h_r = \left(1 - \frac{1}{9.15 + 0.000164 R^{2.875}}\right) h \quad (40)$$

where R is the radius of profile curvature, h is found from Eq. (38), and h_r and R are in mm.

3.2 Model assessment

An analysis of the predictions by the models in Eqs. (38) and (40) with respect to the process parameters in AWJ straight cutting and profile cutting has been carried out to study the models' generality and plausibility, as shown in Figs. 4 and 5 where the lines represent the predicted trends while the symbols shown the experimental results. In general, the trends for the depth of cut with respect to water pressure, nozzle traverse speed, and abrasive flow rate in profile cutting are similar to those in straight cutting, i.e. the depth of cut increases with an increase in water pressure and abrasive flow rate, but decreases with an increase in nozzle traverse speed. In addition, the depth of cut increases with the radius of profile curvature, as shown in Fig. 5(a), so that straight cutting yields a larger depth of cut than profile cutting under the corresponding cutting conditions.

The plotted lines in Fig. 4 show the predicted trends of depth of cut with respect to water pressure and nozzle traverse speed under different abrasive flow rates in AWJ straight cutting. It can be seen that the depth of cut increases almost linearly with water pressure, since a higher water pressure gives higher speeds to the particles which in turn remove more material and generate a deeper slot. In contrast, the depth of cut deceases monotonically with the nozzle traverse speed, as shown in Fig. 4(b), since a faster travelling jet allows less overlapping cutting actions so that fewer particles impinge a given area of the target material, reducing the depth of cut. Fig. 4 also shows that the depth of cut increases with an increase in abrasive mass flow rate, as may be expected from the analysis in the first part of this investigation. For the range of standoff distances tested, the effect of this variable on the depth of cut is negligible as discussed in first part of this study and, hence, is not included in the depth of cut models. Furthermore, it can be seen from Fig. 4 that the experimental data correlates very well with the predicted results. Consequently, it may be stated that the general forms of developed models are reasonable and correct.

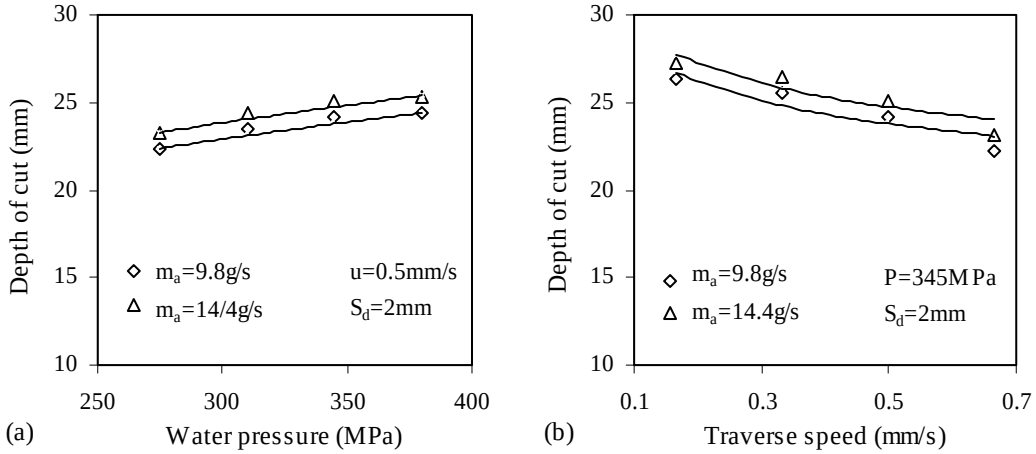

Fig. 4 Predicted trends for the depth of cut in AWJ straight cutting

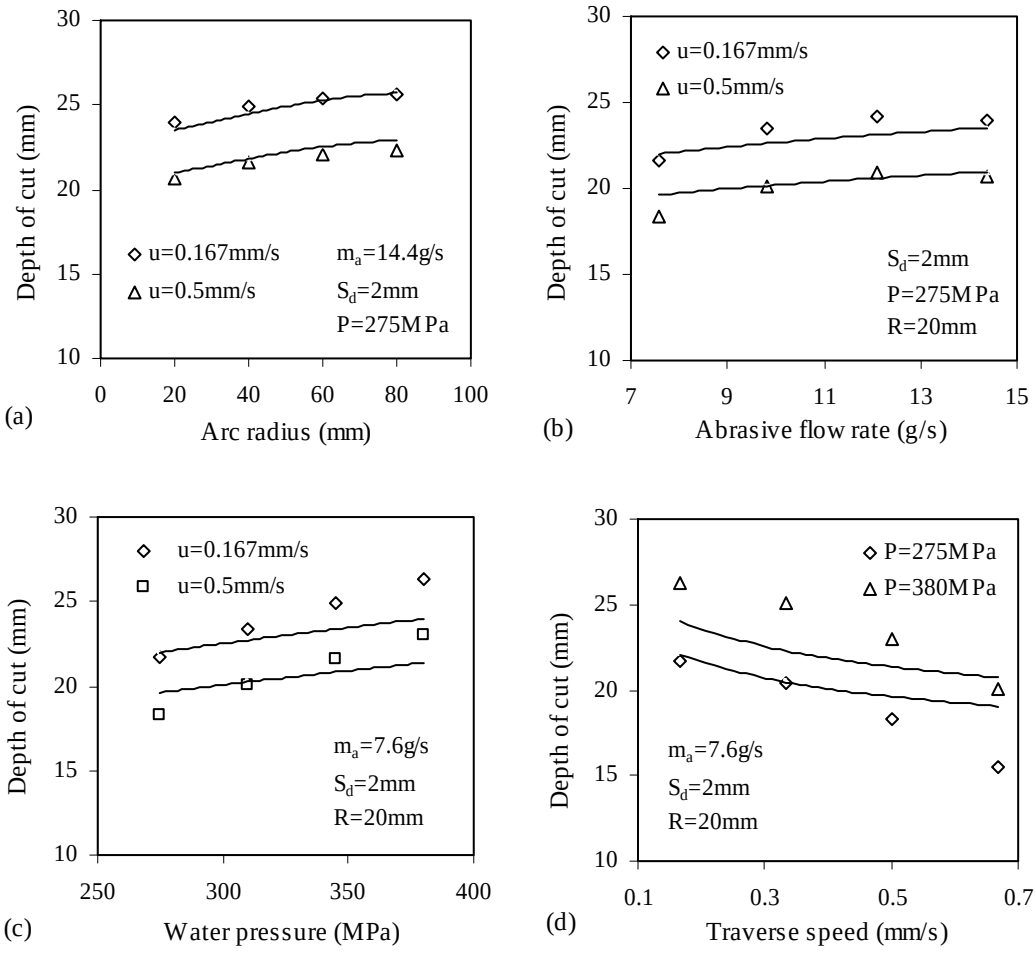

Fig. 5 Predicted trends for the depth of cut in AWJ profile cutting

Fig. 5 shows the relationships between the depth of cut and process variables in profile cutting. It can be noticed that while the predicted trends of the depth of cut with respect to abrasive mass flow rate, water pressure and nozzle traverse speed are similar to those in AWJ straight cutting, an increase in the radius of profile curvature is associated with an increase in the depth of cut. This is consistent with the experimental findings. In general, the predicted results are again in good agreement with experimental data represented by the symbols in the

figure. This qualitative analysis and comparison show that the developed predictive models have been formulated correctly.

Quantitative comparisons between the predicted and experimental data have been carried out to examine the adequacy of the models by using Eq. (16). The histograms in Figs. 6(a) and (b) show the percentage deviations for straight cutting (Eq. (38) and profile cutting (Eq. (40) respectively. It can be found that for straight cutting, the model's prediction gives an average percentage derivation of 0.09% with a standard deviation of 2.79%. For profile cutting, the average percentage deviation is -4.1% and the standard deviation is 7.25%. It may be concluded from these results that the predictive models can yield reasonable and adequate predictions for the depth of cut in AWJ machining of alumina ceramics.

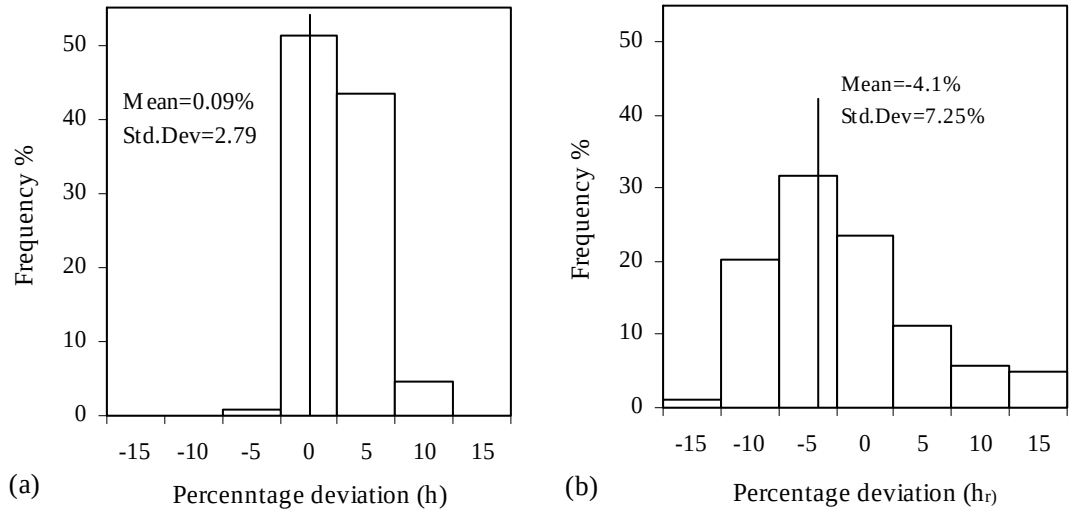

Fig. 6 Percentage deviations of predicted depth of cuts from experimental data:
(a) Straight cutting, (b) Profile cutting

4. EMPIRICAL MODELS FOR OTHER KERF CHARACTERISTICS

At this stage of development, a number of fundamental phenomena in AWJ cutting have not been well understood, so that there are difficulties in mathematically modelling all aspects of the AWJ cutting process, such as the kerf width. To facilitate practical applications, a regression analysis has been carried out to establish empirical models relating top kerf width and smooth depth of cut to the process variables. The models are applicable to both AWJ straight cutting and profile cutting since the kerf curvature has been found to have no significant effect on these two quantities [**1**].

The regression procedure was carried out using an SPSS software package considering the four major process parameters, water pressure, nozzle traverse speed, standoff distance and abrasive mass flow rate. Four different possible models, straight line model, power model, logarithmic model and quadratic model, were tested for top kerf width and smooth depth of cut at a confidence interval of 95%. The coefficients of determination (R^2) for the four possible models are given in Table 1.

Examining the coefficients of determination (R^2) showed that the quadratic models gave the highest R^2 values of 94.7% and 96.2% for the top kerf width and the smooth depth of cut respectively. Thus, a further analysis was made on the quadratic models with interactions.

Table 1 Coefficients of determination of the possible models

	Coefficient of determination (R^2)	
	Top kerf width	Smooth depth of cut
Straight line model	0.911	0.871
Power model	0.900	0.100
Logarithmic model	0.901	0.933
Quadratic model	0.947	0.962

To consider four process parameters, 15 estimated variables are needed to fit a quadratic model and the model is likely to be too complicated for practical use. Thus, the 'backward' elimination procedure was used and the final simplified models for the top kerf width and smooth depth of cut are given by

Top kerf width:

$$\begin{aligned} w_t = &-0.314 + 0.157 m_a + 0.095 S_d + 0.0023 P + 0.012 S_d^{\,2} \\ &- 0.00755 m_a S_d - 0.000223 m_a P - 0.037 m_a u \end{aligned} \tag{41}$$

Smooth depth of cut:

$$\begin{aligned} h_s = &-3.068 + 0.397 m_a + 1.8 S_d + 0.035 P - 14.45 u + 22.3 u^2 \\ &- 0.482 m_a u - 0.0045 S_d P - 0.0235 u P \end{aligned} \tag{42}$$

where w_t is the top kerf width (in mm), h_s is the smooth depth of cut (in mm), m_a is in g/s, S_d is in mm, P is in MPa, and u is in mm/s.

The R^2 values for the two simplified empirical models are respectively 94.1% and 96%. The adequacy of the empirical models are further checked quantitatively based on the percentage deviations of the model predictions from the corresponding experimental results using Eq. (16). These are shown in the histograms in Fig 7. It can be seen that the model predictions for the top kerf width yield an average percentage deviation of 0.4% with a standard deviation of 4.12%. The corresponding deviations for the smooth depth of cut are 0.1% on average and 6.95% for the standard deviation, as shown in Fig. 7(b). Consequently, the empirical models developed can give adequate predictions of these two cutting performance measures for the ranges of conditions used in this study.

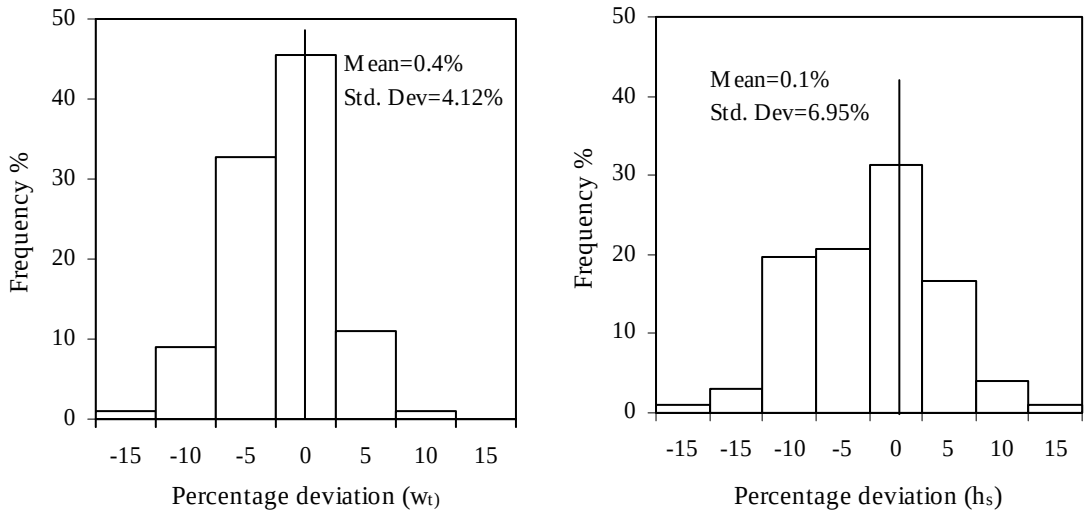

Fig. 7 Percentage deviations of model predictions from the experimental data: (a) Top kerf width, (b) Smooth depth of cut

5 CONCLUSIONS

Predictive models for the major cutting performance measures in AWJ cutting, i.e. the depth of cut, kerf taper angles, top kerf width and smooth depth of cut, have been presented for both straight-slit cutting and profile cutting of an 87% alumina ceramic. The models have been assessed by analysing the predicted trends of the cutting performance measures with respect to the process variables and by comparing with the experimental results. It has been shown that the predictive models can adequately predict the cutting performance measures both qualitatively and quantitatively, and form the essential basis for the effective and optimum use of the AWJ cutting process.

ACKNOWLEDGEMENTS

The authors wish to thank the Australian Research Council (ARC) for financial support to this and other projects.

REFERENCE

1 **Wang, J.** and **Liu, H.** Profile cutting on alumina ceramics by abrasive waterjet. I. Experimental investigation, *Proc. IMechE Part C: J. Mech. Eng. Sci.*

2 **Wang, J.** *Abrasive Waterjet Machining of Engineering Materials*, 2003 (Trans Tech Publications, Uetikon-Zuerich, Switzerland).

3 **Wang, J.** and **Guo, D. M.** A predictive depth of penetration model for abrasive waterjet cutting of polymer matrix composites. *J. Mater. Proc. Technol.*, 2002, **121**, 390-394.

4 **Hashish, M.** and **Du Plessis, M. P.** Prediction equations relating high velocity jet cutting performance to standoff distance and multipasses. *J. Eng. Ind.*, 1979, **101**, 311-318.

5 **Chen, L.**, **Siores, E.** and **Wong, W. C. K.** Kerf characteristics in abrasive waterjet cutting of ceramic materials. *Int. J. Mach. Tools Manufact*., 1996, **36**, 1201-1206.

6 **Hocheng, H.** and **Chang, K. R.** Material removal analysis in abrasive waterjet cutting of ceramic plates. *J. Eng. Ind.*, 1994, **40**, 287-304.

7 **Hashish, M.** and **Hilleke, M.** Water jet machining of composites and ceramics, In *Machining of Ceramics and Composites* (Ed.: S. Jahanmir, M. Ramulu and P. Koshy), 1999 (Marcel Dekker, New York), pp. 427-482.

8 **Isaacson , E. De St. Q.** and **Isaacson, M. De St. Q.** *Dimensional Methods in Engineering and Physics: Reference Sets and the Possibilities of Their Extension***, 1975 (**Edward Arnold, London).

9 **Svobodny, T.** *Mathematical Modelling for Industry and Engineering*, 1998 (Prentice Hall, N.J.).

10 **Evans, A. G.** Impact damage in ceramics. *Fracture mechanics of ceramics*, 1978, **3**, 303-330.

11 **Sheldon, G. L.** and **Finnie, I.** The mechanism of material removal in the erosion cutting of brittle material. *J. Eng. Ind.*, 1966, **88**, 393-400.

12 **Zeng, J.** and **Kim, T. J.** Development of an abrasive waterjet kerf cutting model for brittle materials. In Proceedings of 11th International Conference on Jet Cutting Technology, Bedford, UK, 1992, pp. 483-501.

13 **El-Domiaty, A. A.** and **Abdel-Rahman, A. A.** Fracture mechanics-based model of abrasive waterjet cutting for brittle materials. *Int. J. Adv. Manuf. Tech.*, 1997, **13**(3), 172-181.

14 **Liu, H.** *A Study of the Cutting Performance in Abrasive Waterjet Contouring of Alumina Ceramics and Associated Jet Dynamic Characteristics*, 2004 (PhD thesis, Queensland University of Technology, Brisbane, Australia).

15 **Deam, R. T.**, **Lemma, E.** and **Ahmed, D. H.** Modelling of the abrasive water jet cutting process. *Wear*, 2004, **257,** 877-891.

16 **Hashish, M.** A model for abrasive-waterjet (AWJ) machining. *J. Eng. Mater. Tech.*, 1989, **111**, 154-162.
17 **Hashish, M.** Abrasive-waterjet studies, In Proceedings of 16th International Conference on Water Jetting, Cranfield, France, 2002, pp. 13-47.